Decreasing pores in a laser cladding layer with pulsed current

Deqiao Xie (谢德巧), Jianfeng Zhao (赵剑峰)*, Yongai Qi (戚永爱), Yue Li (李 悦), Lida Shen (沈理达), and Meng Xiao (肖 猛)

College of Mechanical and Electrical Engineering, Nanjing University of Aeronautics and Astronautics, Nanjing 210016, China

**Corresponding author: zhaojf@nuaa.edu.cn*

Received August 15, 2013; accepted October 15, 2013; posted online November 9, 2013

A pulsed current is introduced into the traditional coaxial laser cladding process to decrease the porosity of the cladding layer. The magneto contraction force caused by pulsed current exerted on the molten pool squeezes the gas out and compensates the shrinkage during molten pool solidification. As a result the porosity of the cladding layer is decreased to an extremely low degree. Simultaneously, the grain of the cladding layer is finer with the added supercooling degree with pulsed current. The microhardness of an equiaxed zone in the cross section of a cladding layer also increases.

OCIS codes: 140.3390, 160.3390, 350.3850.
doi: 10.3788/COL201311.111401.

Laser cladding is a burgeoning surface modification technology with properties such as low dilution, high bonding strength and fine solidification structure This technology can promote the surface hardness of a work piece corrosion and wear resistance thus effectively prolonging the service life[1]. Combined with the concept of three-dimensional (3D) printing, laser cladding can also develop into a new technology called laser cladding forming (LCF). This technique can fabricate components with complicated appearances, along with the widely applied category of processing materials and high flexibility. LCF is also capable of realizing gradient function manufacturing and has a die-less, near-net shape[2–5].

However, mechanical properties are typically weakened by pores formed in the laser cladding layer because of trapped gas and shrinkage[6,7]. Gas porosity usually occurs because of a reduction in the solubility limit of gas with decreasing temperature, such as in hydrogen nitrogen or involved gas[8]. Microporosity shrinkage results from lack of feeding in the mushy zone, ie., the increase in density associated with solidification cannot be compensated entirely by fluid flow[9]. Researchers have attempted to decrease porosity in several ways. Chen *et al.*[10] found that gas porosity can be decreased when ultrasonic vibration was introduced into the laser cladding process. Under high-frequency vibration tiny bubbles can gather to form a big bubble that can easily rise out of a molten pool. Zhou *et al.*[11] used induction to stir the molten pool to increase the probability of gas escape. Most methods only decrease gas porosity and studies on diminishing shrinkage porosity are rarely reported.

A new method that applies pulsed current into the molten pool during the laser cladding process is proposed in this letter to decrease shrinkage porosity. The scheme of pulsed current-assisted laser cladding process is shown in Fig. 1. Nakada *et al.*[9,12] believed that pulsed current can generate a powerful contraction force when it flows through liquid metal. The magneto contraction force caused by the current can press the liquid to compensate shrinkage rapidly, thus decreasing shrinkage porosity. The force caused by pulsed current also squeezes the gas out and compensates shrinkage rapidly, thus decreasing gas porosity.

In the present experiment the Ni-based powder of FGH95 was deposited on the substrate of the superalloy GH4169. The size of the powder was between 100 and 150 μm. The compositions of FGH95 and GH4169 are listed in Tables 1 and 2, respectively. In addition, coaxial laser cladding was also used in the experiment.

A series of experiments was conducted with three statuses: cladding with pulsed current, cladding with direct

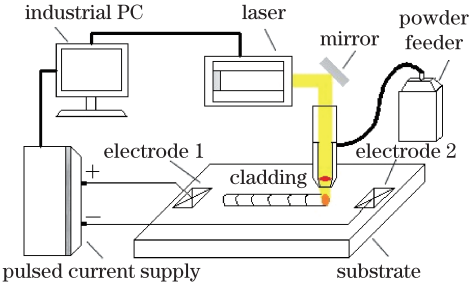

Fig. 1. Schematic of the pulsed current augmented laser cladding process.

Table 1. Composition of FGH95 (wt.-%)

C	Cr	Ni	Mo	Al	Ti	Nb
0.04–0.09	12–14	Bal.	3.3–3.7	2.3–3.7	3.3–3.7	$\leqslant$ 0.015
Cu	Co	Mn	Si	S	P	Fe
3.3–3.7	7–9	$\leqslant$ 0.15	$\leqslant$ 0.2	$\leqslant$ 0.015	$\leqslant$ 0.015	$\leqslant$ 0.5

Table 2. Composition of GH4169 (wt.-%)

C	Cr	Ni	Mo	Al	Ti	Nb+Ta
$\leqslant$ 0.08	17–21	50–55	2.8–3.3	0.2–0.8	0.65–1.55	4.75–5.5
Cu	Co	Mn	Si	S	P	Fe
$\leqslant$ 0.10	$\leqslant$ 1.0	$\leqslant$ 0.35	$\leqslant$ 0.35	$\leqslant$ 0.015	$\leqslant$ 0.015	Bal.

Table 3. Parameters of the Coaxial Laser Cladding

Laser Type	PRC–CO2 Laser
Laser Power (W)	1400
Laser Beam (mm)	3×2 (rectangle)
Scanning Speed (mm/min)	200
Powder Feeder Speed (g/min)	21.4

Table 4. Samples with Related Current Parameters

Sample	I	II	III
Current Type Current	no	direct	pulsed
Value (A) Frequency	–	11	11
(Hz)	–	–	2000
Duty Ratio (%)	–	–	20

current, and cladding without current. The process parameters are listed in Table 3. Accordingly, three typical samples prepared with different current parameters are shown in Table 4.

The microstructure characteristics of the cross sections in the cladding layers were observed using a XJP-300 optical microscope on the polished sections etched with a mixture of 20-ml HNO_3 + 1-ml HF. The microhardness of the cross sections of all the samples was measured by an HXP-1000TM microhardness tester with a load of 500 N and a dwell time of 10 s.

In Fig. 2, the white and black dots in the cross sections perpendicular to the scanning direction are all pores. Numerous pores are observed in the cross sections, as shown in Figs. 2(a) and (b). Many of these pores occur in the upper part of the cladding layer. By contrast, few pores are found in Fig. 2(c). Moreover, Fig. 2(d) shows that distinct pores occurred in the cladding layer. The pores may also have rounded boundaries, such as pore A. However, pore B has an irregular shape.

The round shape of pore A suggests that this pore was formed as a result of gas evolution during the laser cladding process[13]. Some gases functioning as powder carriers probably rushed into the molten pool during the laser cladding process. However, not all of the gases had enough time to escape from the molten pool because the solidification velocity was fast. The gases in the upper part of the molten pool might have time to escape. Most of the gases in the bottom half did not have enough time to rise out of the molten pool. Hence a significant amount of pores were bounded in the upper part of the cladding layer, as shown in Fig. 2(a). Meanwhile, the irregular boundary of pore B might have been caused by shrinkage resulting from lack of feeding.

However the difference in sample I when sample III was prepared is that pulsed current flowed through the molten pool. The carrier has a tendency to move toward the center axis under the magnetic field generated when the electric current flows through the conductor. This process is called "magneto contraction". Liquids or solids that are easily deformed may change their appearances with the action of the magneto contraction force the existence of which has been proven by He *et al.*[11,14]. Moreover He *et al.* found that the force generated by pulsed current increased with the increase in current density.

Considering the skin effect of the pulsed current, most carriers gather beyond the skin of the conductor. Otherwise the relationship between current density $J(x)$ and distance to skin x is shown as

$$J(x) = J_s \exp(-t/\delta), \tag{1}$$

where J_s is the current density of the skin, and δ represents the depth of the skin effect, which is a coefficient of the resistance of the conductor and the frequency of pulsed current. Even a minimal variation in x can make $J(x)$ distinct thus leading to different pressures.

As a result, the gas can be squeezed out under pressure because the inner molten pool is liquid. The pores caused by lack of shrinkage can be compensated swiftly during solidification. Hence porosity can be eliminated significantly, such as in sample III as shown in Fig. 2(c).

In the absence of the skin effect in sample II the magneto contraction force generated by the direct current may be feeble because of its weak electricity flow. The schematic diagram of the electricity flow in samples II and III is shown in Fig. 3. Thus, the flow driven by the magneto contraction force with direct current may not be as intense as that with pulsed current. The porosity in sample II is not less than in sample I.

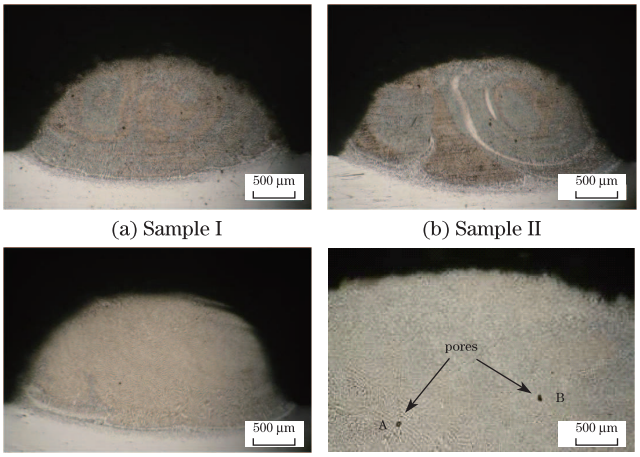

(a) Sample I (b) Sample II

(c) Sample III (d) Pores in the cladding layer

Fig. 2. Images of the sample cross sections.

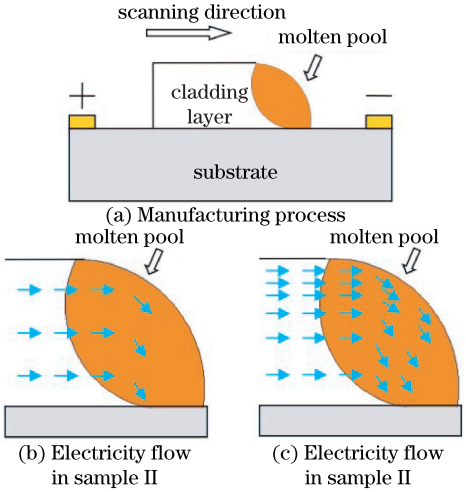

(a) Manufacturing process

(b) Electricity flow in sample II (c) Electricity flow in sample II

Fig. 3. Schematic diagram of the electricity flow.

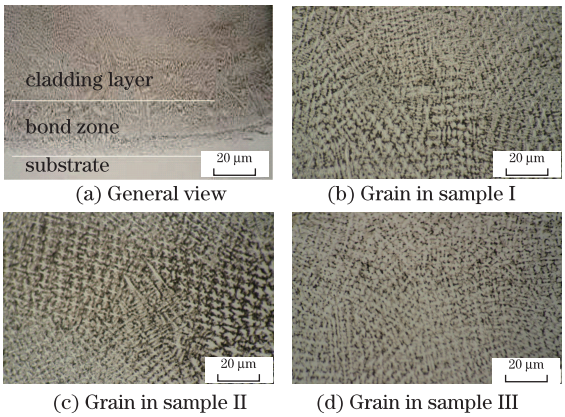

(a) General view (b) Grain in sample I

(c) Grain in sample II (d) Grain in sample III

Fig. 4. Grain features of the sample cladding layers.

The grain features of the cladding layers of the samples are presented in Fig. 4. As shown in Fig. 4(a) the bond zone nearly consists of dendrite growing perpendicular to the interface of the substrate and bond zones. Most of the cladding layers are made up of isometric crystals. As shown in Fig. 4(d), sample III has smaller grains with a more uniform distribution compared with sample II which, in turn, has thicker grains than sample I. The primary dendrite arm spacing (PDAS) also decreased from approximately 5 to 3.3 μm with pulsed current By contrast, under the influence of direct current, the PDAS was enhanced to approximately 6 μm, which is larger than that in sample I.

The dendrite growth orientation is against the heat flow direction[15]. By contrast, the growth of the isometric is along the heat flow direction. Given that the nucleation in the bond zone was heterogeneous and the substrate was colder than the molten pool during laser cladding, the dendrite growth direction pointed toward the direction of the cladding layer. Inversely, a large amount of homogeneous nucleation occurred in the molten pool for supercooling. Therefore, the cladding layer during solidification consists of the isometric with a trend toward the substrate.

With the aid of pulsed current the cladding layer in sample III consists of tinier isometrics than those in sample I. According to the Avrami equation, tinier grains can be achieved with the increase in nucleation rate which is significantly affected by the degree of supercooling ΔT. In a conventional solidification process, the degree of supercooling is called ΔT which is closely related to the cooling speed. Pulsed current can provide a beneficial ΔT_{p} added to the degree of supercooling in conventional solidification[16]. The influence is described as

$$\Delta T_{\mathrm{p}} = \mathrm{k}\mathrm{J}_0^2 \xi \pi r^2 \Delta V T_{\mathrm{m}} c^{-1}, \tag{2}$$

where k is a constant related with the spherical coordinates θ, J_0 is the current density and before nucleation; $\xi = \sigma_1 = \frac{\sigma_1 - \sigma_2}{\sigma_2}$, σ_1 is the conductivity of the nucleus whereas σ represents the conductivity of the parent phase; ΔV is the volume of nucleation and r is the radius of the sphere. In addition, T_{m} is the temperature of the fusion point, and c represents specific heat capacity.

However the joule heat under the electric field is equal to the inner heat source in the solidification system, thus decreasing the cooling rate. The increase in temperature caused by the joule heat is demonstrated as

$$\Delta t = J_0^2 \rho_{\mathrm{e}} \tau_{\mathrm{p}} / \rho c, \tag{3}$$

where ρ_{e} is the electrical resistivity and τ_{p} is the current pulse width; ρ represents the density of the molten pool References[17] demonstrate that the increase in τ_{p} can cause temperature rise, which is not conductive to nucleation. Moreover, a short τ_{p} can avoid an unfavorable situation.

Given that the cooling rate of conventional laser cladding ranges from 10^3 to 10^4 K/s, and the melting cooled from approximately 2000 (the temperature near the edge of the molten pool) to 1500 K (melting point) solidification time may last form 5 to 50 ms. Given that the pulse cycle is 0.5 ms, pulsed current can act on the solidification process for at least one cycle. When the current is on a high level ΔT_{p} caused by pulsed current can enhance the degree of supercooling. Simultaneously the joule heat with an opposite effect on solidification also exists. However, when the current is on a low level, the previously generated joule heat is dispersed because of the heat conduction. The time for the duty ratio is only 20%. Therefore pulsed current promotes the nucleation rate with respect to the entire cycle.

Nevertheless, given that τ_{p} can be regarded as a long pulse width when sample II was processed, the joule heat continuously increases the temperature. Thus, the degree of supercooling probably declines. The grain in sample II is not as small as that in sample I because of the decrease in nucleation ratio.

The microhardness of the equiaxed zone in the cross sections of the cladding layers in all samples has been detected and the results are shown in Fig. 5.

With the same grain component, microhardness is influenced by grain size and distribution. As demonstrated in Fig. 5, microhardness is increased with pulsed current hence the grain in sample III becomes more compact than that in sample I. Microhardness can also be improved to a certain extent because less pores appear in sample III. Compared with pulsed current direct current has an opposite role in the laser cladding layer. The grain in sample II is not as intensive as that in sample I because of the decrease in nucleation rate and the existence of numerous pores.

In conclusion, in this experiment pulsed current and direct current are applied to a traditional coaxial laser cladding separately. Porosity decreases to an extremely low degree with the aid of pulsed current. The magneto contraction force exerted on the molten pool squeezes the gas out and compensates shrinkage swiftly. The magneto contraction force could be enhanced to a certain extent by the skin effect. Moreover, fine grain is observed in the cladding layer of sample III with the increase in

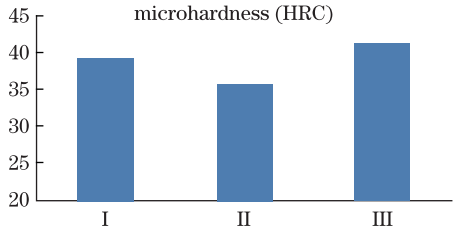

Fig. 5. Microhardness values of the samples

nucleation rate. With more compact grains and minimal porosity, microhardness is elevated in the cladding layer of sample III. However direct current is not beneficial to decrease porosity during laser cladding because only minimal current flowed through the molten pool. Even worse grain size increases because joule heat decreases the degree of supercooling during solidification. The microhardness of the equiaxed zone in the cross section of sample II is less than that in sample I because of the decrease in nucleation rate and the existence of numerous pores.

This work was supported by the National Natural Science Foundation of China (No. 51205198) the Aviation Science Foundation (No. 2011ZA52007) the Special Funding for Basic Research for Central Universities (No. 30820122011ZA52007) and the Innovation Foundation for Graduates of the Nanjing University of Aeronautics and Astronautics (No. kfjj120216).

References

1. Y. Huang, Y. Yang, G. Wei, W. Shi, and Y. Li, Chin. Opt. Lett. **6,** 356 (2008)
2. J. Song, Y. Li, Q. Deng, AND D. Hu, J. Mech. Eng, **46,** 29 (2010)
3. H. Tan, F. Zhang, J. Chen, X. Lin, and W. Huang, Chin. Opt. Lett. **9,** 051403 (2011)
4. Y. Liu, J. Chen, Q. Zhang, L. Xue, X. Lin, and W. Huang, Chin. Opt. Lett. **9,** 071402 (2011)
5. Q. Nadeem and S. J. Na, Chin. Opt. Lett. **11,** 021402 (2013)
6. S. Dsdbakhsh, L. Hao, and N. Sewell in *Proceedings of the 10^{th} National Conference on Rapid Design, Prototyping and Manufacturing*, 53 (2009)
7. L. Hao, and S. Dsdbakhsh. Chinese J. Lasers **36,** 3192 (2009)
8. A. Nickel, D. Barnett, and P. F, Mater Sci. Eng. A **317,** 59 (2001)
9. ASM Handbook, *Powder Metal Technology and Applications* (ASM International 1998)
10. C.-Y. Chen, Q.-L. Deng, and J.-L. Song, Trans. Nanjing Univ. Aeron. Astron. (in Chinese) **37** (suppl.), 44 (2005)
11. S.-F. Zhou, Y.-J. Huang, X.-Y. Zeng, and Q.-W. Hu, Mater Sci. Eng. (A) **480,** 564 (2008)
12. M. Nakada, Y. Shiohara, and M. C. Flemings, ISIJ International **30,** 27 (1990)
13. J.-L. Huang, N. Warnken, Jean-Christophe Gebelin, Martin Strangwood, and Roger C. Reed, Acta Mater **60,** 3215 (2012)
14. S.-X. He, J. Wang, B.-D. Sun, and Y.-H. Zhou, Chin. J. Nonfer. Met. **12,** 173 (2002)
15. X.-Q. Bi, X.-J. Hu, and J. Wang, J. Aeron. Mater **29,** 45 (2009)
16. J. P. Barnak, A. F. Sprecher, and H. Conrad, Scripta Metall **31**, 1691 (1995)
17. R.-S. Qin, H.-C. Yan, G.-H. He, and B.-L. Zhou, Chin. J. Mat. Res. **9,** 219 (1995)